Chapter 4

Immunosuppressive Drug Sensor based on MoS_2-Polycarboxyindole Modified Electrodes

4.1 Introduction

Azathioprine (Azp) is associated with a chemical category of purine analogues named 6-[(1-methyl-4-nitroimidazole-5-yl) thio] purine. Azp is an immunosuppressant and antileukemic drug that finds contemporary applications in various disorders such as ulcerative colitis, rheumatoid arthritis, Crohn's disease, and pemphigus [Rae et al., 2016; Asadian et al., 2016]. Mercaptopurine is the active form of Azp which acts by decreasing the reactions of T and B cells by inhibiting their proliferation [McLeod and Siva, 2002]. Continued exposure to Azp for a long time may lead to the development of specific types of cancer like skin cancer, blood cancer, and lymphoma and with some serious side effects including hair loss, nausea, fatigue, and rash. To counter these issues, it is crucial to evolve an accurate and sensitive method for the routine and careful monitoring of Azp in clinical operations [Dervieux and Boulieu, 1998; Muller, 2004]. In the past, various techniques have been applied, for instance, high-performance liquid chromatography (HPLC) [Fazio et al., 2007; Tsutsumi et al., 1992], UV-Visible spectrophotometry [Lakshmi and Reddy, 1998; Chalmers, 1975], ^{1}H-NMR spectroscopy [Göger et al., 1999], chemiluminescence [Wang et al., 2012; Govindasamy et al., 2017], ultra-performance liquid chromatography [Davadra et al., 2011], high-performance thin layer chromatography [Kulkarni et al., 2014], flow injection analysis [Wang et al., 2012], surface-enhanced Raman spectroscopy [Chen et al., 2003], capillary zone electrophoresis [Shafaati and Clark, 2000], titrimetry [Sastry et al., 1996] for the determination of Azp in human blood. Although all these techniques are accurate, some of them suffer from various demerits like low sensitivity and selectivity, expensive instrumentation, high cost, time-consuming operation, and

cumbersome extraction procedure with complex and tedious sample pre-treatment that makes them inappropriate for regular analysis in many cases. Analytical and electrochemical measurement techniques play a critical role in biological recognition, environmental monitoring, and drug estimation in human body fluids as well as pharmaceutical formulations. The modern electrochemical methods have an important role in these fields because they have come up with sensational advantages like broad linear dynamic range, high sensitivity, and selectivity, simplicity, short analysis time, and cost-effectiveness with real-time monitoring [Tiwari et al., 2015; Baghbamidi et al., 2016; Tajik and Beitollahi, 2019]. CV and DPV have enjoyed significant interest since they can be used for elucidation of redox electrode process and estimation of trace level amounts of electroactive analytes respectively [Meng et al., 2012; Rashed et al., 2021. The electroreduction of Azp on bare GCE displays an inadequate and wide signal unveiling high overpotential magnitude. Also, this involves very slow electron transfer kinetics [Shahrokhian and Ghalkhani, 2010]. These issues can be addressed and the electrode kinetics can be enhanced through surface modification using a mediator which can fasten the transfer of electrons thereby amplifying the sensitivity and selectivity of the analysis. To serve this purpose, nanostructured materials like nanoparticles [Mehrabi et al., 2021; Alkahtani et al., 2022], nanosheets [Guo et al., 2010; Nikhil et al., 2021; Immanuel and Sivasubramanian, 2020], nanotubes [Guan et al., 2020; Ostovar et al., 2021], etc. present themselves as promising candidates due to their small dimension and size with shape-dependent properties [Regiart et al., 2013; Gedda et al., 2014]. Recently, 2D layered nanomaterials like graphene, TMDs, and other analogues have attained great privilege towards application in the field of electrochemistry. MoS_2 categorizes a typical 2D TMD, which can be easily exfoliated to a few layers because of the weak van der Waals interactions. MoS_2 shows several properties similar to

graphenes like easy functionalization, large surface area, good mechanical strength, and easy storage. Owing to these properties, MoS_2 has found wide applications in the field of electronic devices, electrochemical sensors, catalysis, energy storage [Zhang et al., 2016; Zhang et al., 2019; Zeng et al., 2021; Upadhyay et al., 2016; Zhang et al., 2017; Gan et al., 2017]. For augmenting the electrical, thermal, and mechanical properties, MoS_2 is further modified with different metal nanoparticles, carbonaceous materials, and conducting polymers [Sha and Bhattacharyya, 2020; Wang et al., 2021]. Among them, conducting polymers are an excellent choice of materials for modification because of their low cost, commendable conductivity, and rapid redox kinetics [Fadil et al., 2019]. But only a few works have been reported on the modification of MoS_2 with conducting polymers [Selvam et al., 2021; Tang et al, 2014; Raju et al, 2021; Mishra et al, 2017]. Among conducting polymers, PIn is a promising material to serve the purpose of electrode materials since it combines the properties of polyphenylene and polypyrrole. They display advantageous properties like low toxicity, high redox activity, high thermal stability, fast electrochromic response, and great environmental stability. In addition, CPIn displays a unique property of pH-dependent self-doping due to the presence of COO^- and demonstrates rapid electron transfer [Joshi et al., 2010].

In the current study, MoS_2 has been synthesized using a simple one-step hydrothermal process that provides good control over size and morphology. These MoS_2 nanosheets were further exfoliated in an aqueous medium using monomer 5-carboxyindole (5CIn) without any aid from hazardous solvents and chemicals. These exfoliated nanosheets were exploited as templates for the controlled polymerization of 5CIn using ammonium persulphate (APS). The as-prepared CPIn stabilized MoS_2 nanosheets (MoS_2-CPIn) composite was characterized by numerous techniques, for

instance, FTIR, XRD, SEM, TEM, EDAX, and their electrochemical properties were investigated by voltammetry. MoS_2-CPIn showed commendable electrocatalytic activity and is therefore used as a nano mediator over the GCE surface for electrochemical sensing of immunosuppressive drug Azp. The work demonstrates a simple, sensitive, selective, and low-cost sensory platform with a large surface area for trace-level detection of Azp.

4.2 Experimental Section

4.2.1 Chemicals and Materials

Azp, 5CIn, APS ($(NH_4)_2S_2O_8$), L-cysteine ($HO_2CCH(NH_2)CH_2SH$), sodium molybdate dihydrate ($Na_2MoO_4.2H_2O$), conc. HCl, sodium dihydrogen phosphate (NaH_2PO_4), disodium hydrogen phosphate (Na_2HPO_4) were purchased from Merck, India. Chemicals used in the interference study i.e. L-ascorbic acid, cholesterol, creatine, DA, glucose, glycine, UA, and urea were procured from Sisco Research Laboratories Pvt. Ltd., India. The 0.1 M PBS was formulated by intermixing NaH_2PO_4 and Na_2HPO_4. DI water was utilized in every preparation and experiment. The human blood samples were collected from Sir Sundar Lal Hospital, BHU for Azp detection in human blood serum.

4.2.2 Preparation of MoS_2 nanosheets

A one-step reaction was employed in a hydrothermal autoclave reactor for synthesizing MoS_2 nanosheets (MoS_2) (Figure 4.1) [Mishra et al., 2017]. Cysteine (0.5 g) and sodium molybdate dihydrate (0.25 g) were added to DI water (25 mL) in different beakers and constantly stirred for 30 min to get a complete homogenous solution. Then, both the solutions were intermixed and agitated well for 30 min with temperature maintained at ~40°C, and conc. HCl was added to maintain the pH at 3. The prepared reaction mixture

was introduced into a stainless-steel Teflon-coated autoclave (100 mL) and retained at 200°C for ~42 hours. The reaction mixture was further cooled down to RT, and the dark brown precipitate was obtained by centrifugation. The product was washed with DI water 4-5 times repeatedly followed by washing with ethanol and the product was finally vacuum dried at 80 °C overnight.

As per the previous reports [Mishra et al., 2017], a plausible mechanism for the synthesis of MoS_2 nanosheets has been presented highlighting the catalytic role of H^+ ions. Further, the highly acidic condition nullifies the formation of molybdenum oxides thus favouring the formation of MoS_2. Overall, it is a complex reaction that can be mainly categorized into four steps namely,

i. Hydrolysis of L-cysteine

$$HO_2CCH(NH_2)CH_2SH + H_2O \longrightarrow CH_3COCOOH + NH_3 + H_2S \quad \text{(Eq. 4.1)}$$

ii. conversion of MoO_4^{2-} to MoO_xS_{4-x}

$$MoO_4^{2-} + HS^- \longrightarrow MoO_4S_{4-X} + H_2O \quad \text{(Eq. 4.2)}$$

iii. acid-catalyzed formation of MoS_3

$$MoO_4S_{4-X} + H^+ \longrightarrow MoS_3 \quad \text{(Eq. 4.3)}$$

iv. formation of MoS_2 nanosheets

$$MoS_3 \longrightarrow MoS_2 \quad \text{(Eq. 4.4)}$$

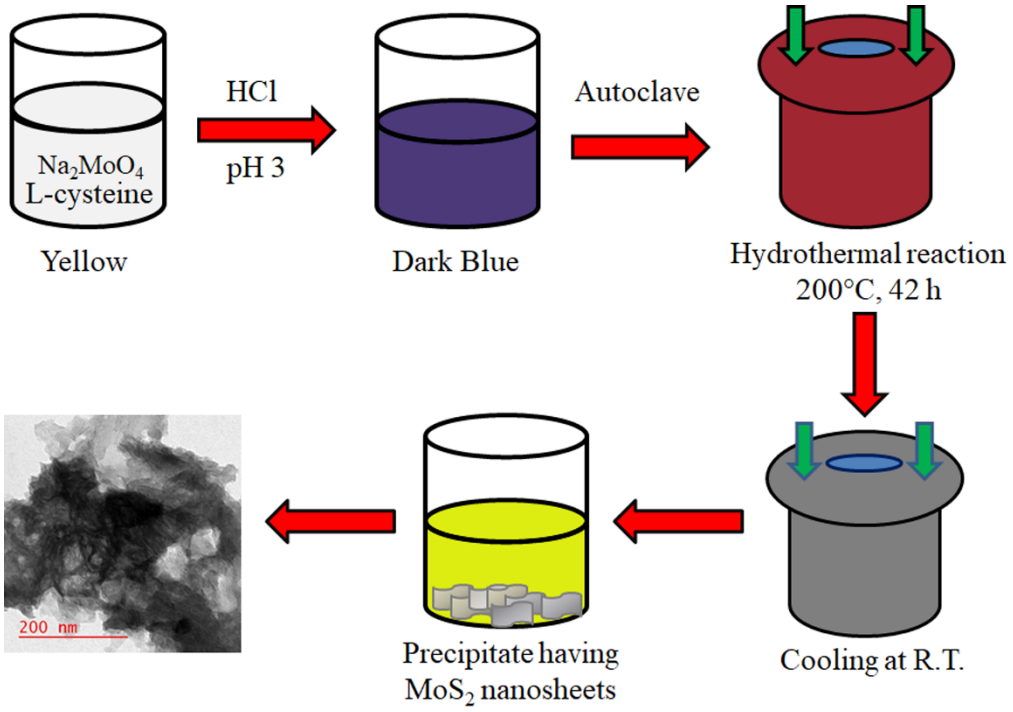

Figure 4.1 Schematic presentation of synthesis of MoS_2 nanosheets using hydrothermal technique.

4.2.3 Synthesis of MoS_2-CPIn composite

MoS_2-CPIn composite has been synthesized as per the reaction scheme shown in Figure 4.2. For that, 10 mg of synthesized MoS_2 nanosheets were suspended in 10 mL 0.1 N HCl and sonicated properly to achieve uniform distribution. 20 mg of 5CIn monomer was solubilized in a minimum amount of ethanol and was mixed dropwise in MoS_2 suspension. The mixture was constantly stirred for 1 h, further sonicated using probe sonication so that monomer gets completely adsorbed over nanosheets and further stacking of nanosheets gets restricted. 28.32 mg APS was dissolved in 0.1 N HCl (5 mL). This solution was mixed dropwise in the prepared suspension with subsequent stirring for polymerization. The reaction was then kept in the refrigerator overnight. After 24 h, the precipitate was extracted by centrifugation at 5000 rpm and washed three times with ethanol to eliminate the unreacted monomer. Later, the product was vacuum dried at 60°C and preserved in the desiccator.

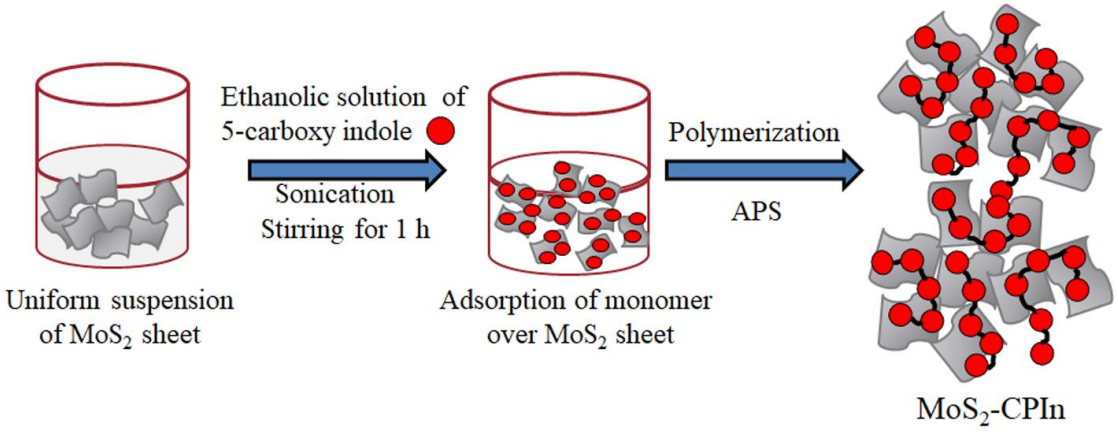

Figure 4.2 Schematic illustration for the exfoliation of MoS_2 nanosheet and synthesis of MoS_2−CPIn nanocomposite.

4.2.4 Electrode fabrication

Initially, the GCE with a diameter of 3 mm was cleaned by polishing it in 0.3 µm alumina slurry. Further, it was undergone through 2 min sonication in DI water followed by acetone three times and dried in a desiccator. The MoS_2-CPIn composite (1.0 mg) suspension in DI water (1 mL) was sonicated for 1 h to yield a homogeneous suspension. Further, 5 µL of prepared ink was used to modify the polished GCE surface by using the drop-casting technique and followed by vacuum drying in a desiccator. MoS_2-CPIn acts as a good electrode modifier because they are negligibly soluble in water so the factor of leaching of the material from the electrode surface can be eliminated.

4.3 Results and Discussion

4.3.1 Structural investigation

The crystallographic nature of the as-synthesized composite was examined through the XRD technique. The XRD measurements of CPIn, MoS_2 and MoS_2−CPIn composite are demonstrated in Figure 4.3(a). Pure CPIn displayed diffraction peaks with characteristic weak reflections between 15−30° [Mishra et al., 2017]. MoS_2 showed XRD signals positioned at 2θ = 13°, 33°, 35°, 44° and 58° which may be observed due to the presence of (002), (100), (103), and (110) planes which are directly related to MoS_2 hexagonal phase (JCPDS No. 37−1492) [Mishra et al., 2017; Joshi and Prakash, 2013]. MoS_2-CPIn composite shows the signature of both CPIn and MoS_2 and has diffraction peaks with decreased intensity and increased FWHM due to the growth of the polymer over the MoS_2 sheet that restricts restacking of the sheet, this fact is well supported by TEM analysis (Figure 4.3(g-i)). The star (*) in the XRD spectra indicates the peak corresponding to the glass which was used as a substrate for recording spectra.

FTIR spectroscopy has been done for the structural investigation of CPIn, MoS_2, and MoS_2-CPIn. Figure 4.3(b) depicts the FT-IR spectra of CPIn, MoS_2, MoS_2-CPIn. MoS_2 exhibits signals at 1612 and 1673 cm^{-1} that correspond to in-group deformation of NH_2 and -C=O vibrational stretching (due to L-cysteine used as a reactant in hydrothermal synthesis), and the peak observed at 1407 cm^{-1} can be accredited to the asymmetric N–C–N vibrational stretching mode. The O–H stretching vibration band appeared at 1185 cm^{-1} and the vibrational peak appeared at 1108 cm^{-1} corresponding to the C–O–H stretching vibration. The C-S vibration stretching is detected at 899 cm^{-1}. A small peak is observed near 670 cm^{-1} which reflects Mo–S vibration [Khawula et al., 2016]. The CPIn exhibits a characteristic peak for aromatic rings at 765 cm^{-1} (corresponding to C-

H bond out of plane deformation in the benzene moiety), 1228 cm^{-1} with 1677 cm^{-1} (representing the distinguishing absorption peak for -C-O and -C=O corresponding to the vibration stretching modes of -COOH), 1377 cm^{-1} (assigned to C-O-H bonds in the plane shearing mode of vibration), 1612 cm^{-1} (vibrational stretching of -C=C group present in indole ring) [Joshi and Prakash, 2013]. The characteristic vibrational peaks for both Mo–S and CPIn are consistently observed in the MoS_2-CPIn composite.

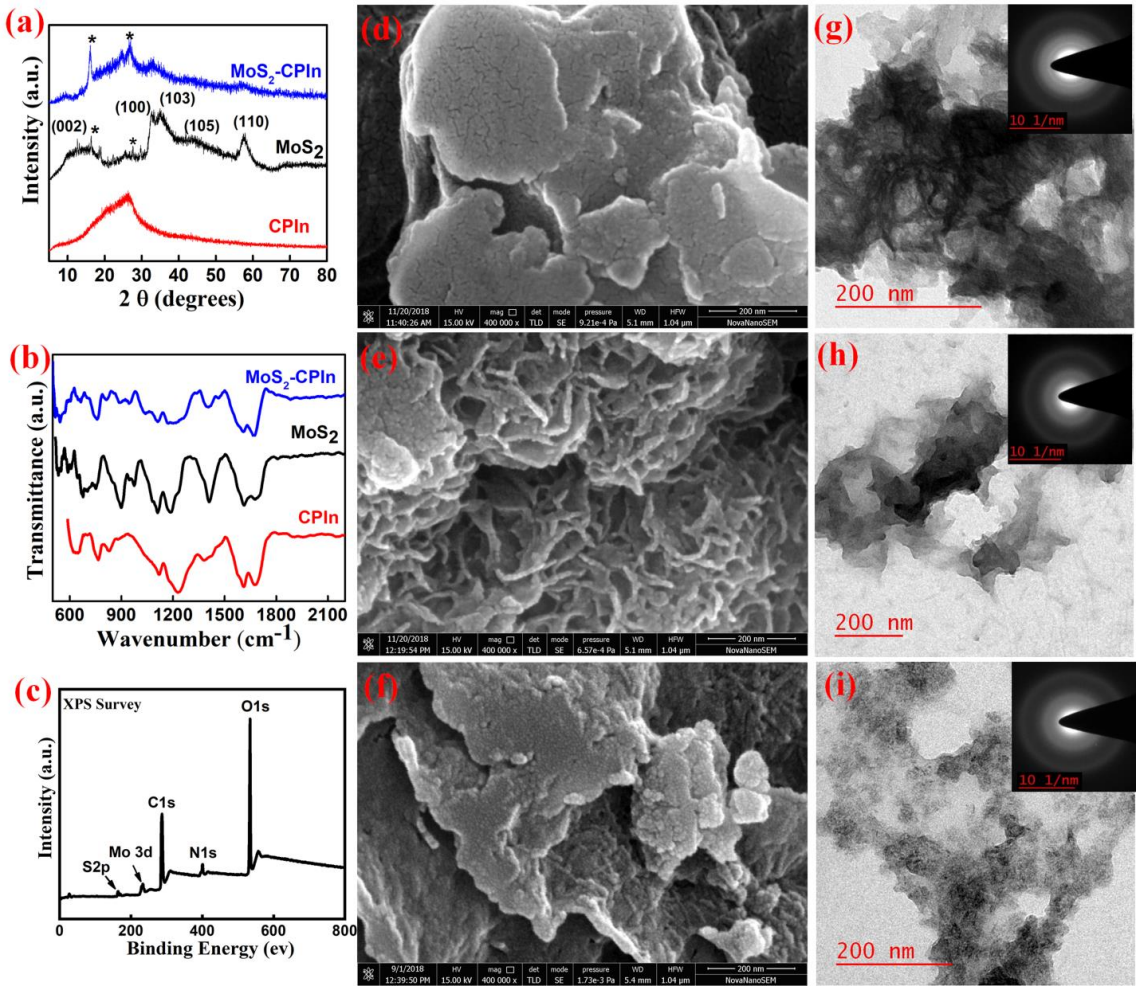

Figure 4.3 (a) XRD spectrum of MoS_2, CPIn and MoS_2-CPIn, (b) FTIR spectra of MoS_2, CPIn and MoS_2-CPIn, (c) XPS survey spectrum corresponding to MoS_2-CPIn (d) displays the SEM image related to CPIn, (e) MoS_2 and (f) MoS_2-CPIn, (g) TEM micrograph of MoS_2, (h) CPIn and (i) MoS_2-CPIn, Inset of g-i shows SAED pattern.

The elemental composition of synthesized MoS_2-CPIn was investigated using XPS. Figure 4.3(c) depicts the XPS survey of MoS_2-CPIn signifying the existence of all elemental compositions. Figure 4.4 (a) shows the C 1s XPS spectrum of MoS_2-CPIn that may be deconvoluted into four peaks: 284.8 eV, 286.8 eV, 288.8 eV, 290.7 eV designated to C–C/C=C, C=N, C–N and (O–C=O) respectively signifying various kinds of carbon present in the composite. Figure 4.4(b) shows the XPS spectrum of N 1s with a prominent signal at 399.9 eV which corresponds to the pyrrolic N (5CIn) in the composite [Han et al., 2014; Wang et al., 2017].

Figure 4.4(c) displays the XPS spectrum of O 1s which may be deconvoluted into two peaks at 533.2 eV (C-O) and 531.6 eV (C=O) designating two different types of oxygen present [Xing et al., 2016]. The XPS spectrum of Mo 3d region (Figure 4.4(d)) may be further deconvoluted into 6 peaks. The XPS signal at 226.7 eV is designated to S 2s of MoS_2 and an intense peak is observed for Mo (IV) $3d_{5/2}$ and Mo (IV) $3d_{3/2}$ binding energies at 228.8 eV and 232.0 eV respectively. Short peaks observed at 233.2 eV and 235.9 eV are designated to Mo $3d_{5/2}$ and Mo $3d_{3/2}$ of Mo (VI) indicating that Mo (IV) is partially oxidized to Mo (VI) during hydrothermal-assisted preparation of MoS_2. Figure 4.4(e) shows a deconvoluted XPS spectrum related to the S 2p peak. The signal examined at 163.7 eV corresponds to S $2p_{1/2}$ and the signal at 161.8 eV is the signature of S $2p_{3/2}$ for S^{2-} [Zhao et al., 2017; Briggs et al., 1981]. The morphology of the developed composite MoS_2-CPIn was assessed using SEM. Figure 4.3(d) represents the SEM micrograph of CPIn designating sheet-like morphology. Figure 4.3(e) shows the pure MoS_2 having flower-like morphology, consisting of interlaced nanosheets. SEM image reveals that the MoS_2 nanosheets are well rough, porous, and scattered. Figure 4.3(f) shows the growth of the CPIn chain in between and over the MoS_2 sheets. MoS_2 sheets provide a good structural

substrate for the growth of CPIn polymer chains. TEM micrographs of MoS_2 (Figure 4.3(g)), CPIn (Figure 4.3(h)) and MoS_2-CPIn (Figure 4.3(i)) were used to demonstrate the internal nature of the developed composite. MoS_2 nanosheets are covered by homogeneously distributed CPIn chains and these chains are very well anchored on the nanosheets. So, the TEM study strongly supports the composite formation. SAED pattern displays the ring-like structure which confirms the polycrystalline nature of the MoS_2 nanosheets.

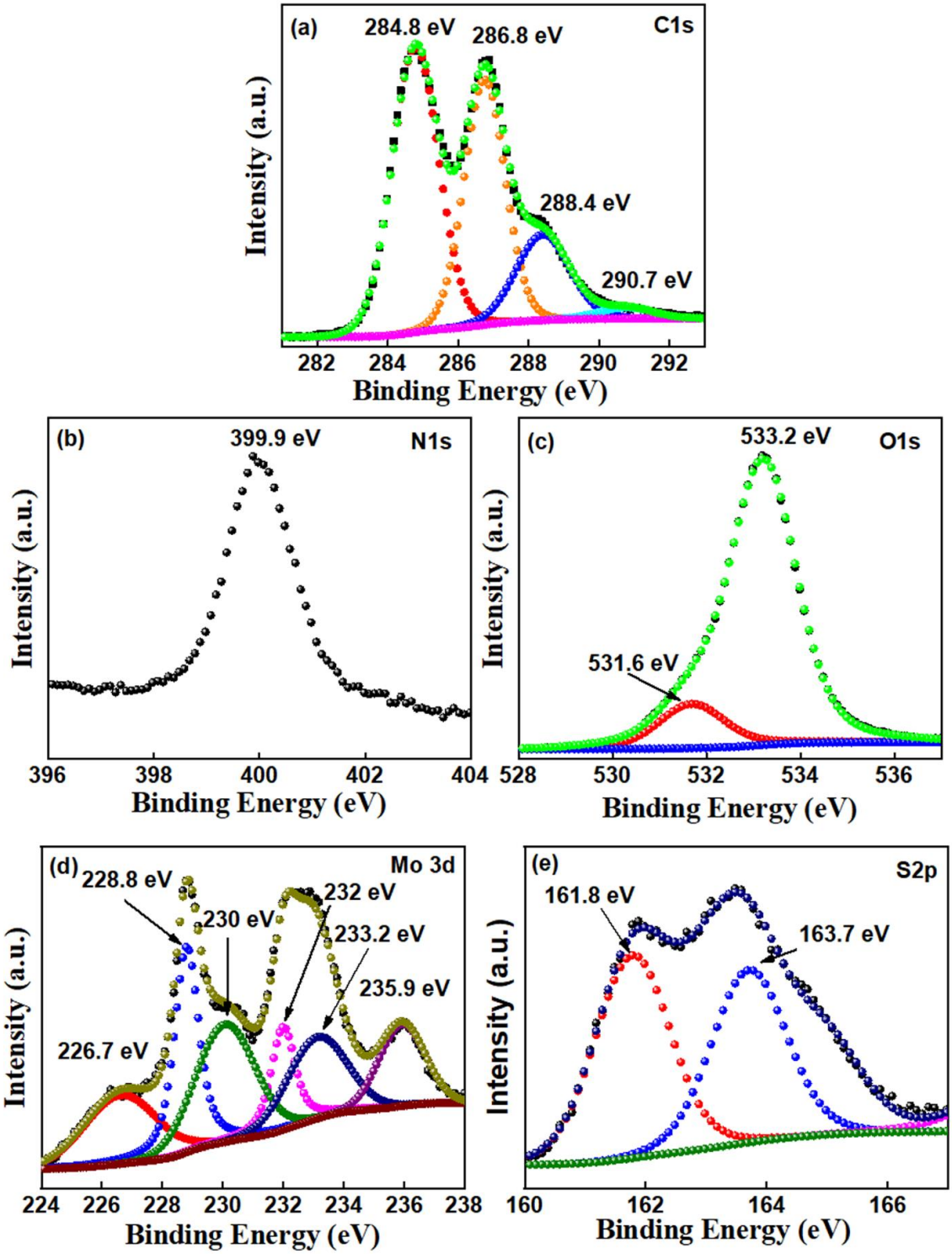

Figure 4.4 XPS spectra of MoS_2-CPIn. (a) C 1s, (b) N 1s, (c) O 1s (d) Mo 3d and (e) S 2p respectively.

4.3.2 Electrochemical Sensing of Azathioprine

4.3.2.1 Electroanalytical response of Azp at MoS_2-CPIn/GCE

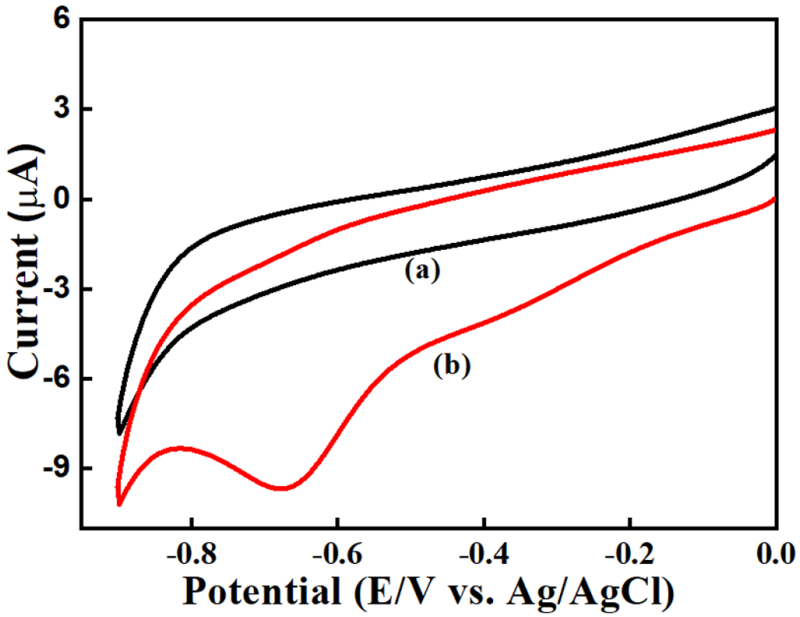

Figure 4.5 CV curves of Azp (9.9 µM) in 0.1 M PBS of pH 7.4 (a) without Azp and (b) with Azp at MoS_2-CPIn/GCE

Azp is an aromatic compound that is electroactive due to the presence of a nitro group (-NO_2). CV of 9.9 µM Azp was recorded on modified MoS_2-CPIn/GCE in 0.1 M PBS of pH 7.4 from 0.0 to -0.9 V potential window at a scan rate of 50mVs^{-1} (Figure 4.5) to investigate the electrochemical response of Azp. MoS_2-CPIn coated GCE, Pt electrode, Ag/AgCl were selected as WE, AE and RE respectively. A sharply defined cathodic peak was observed at -0.656 V in the forward scan and a small anodic peak was found at -0.563 V during the reverse scan. The cathode peak can be attributed to the nitro group (-NO_2) reduction to hydroxylamine (-NHOH) which is irreversible and anodic peak can be assigned to the reversible conversion of the hydroxylamine group to nitroso group as shown in the equation given in Equation 4.5 and 4.6 [Shahrokhian and Ghalkhani, 2009]. The electrochemical reduction of the nitro group involves complex mechanisms and the cathodic peak is ascribed to the 4-electron process in which the nitro group is

reduced to hydroxylamine group (-NHOH). This is in accordance with previously reported works on the electro-reduction of nitro aromatic compounds. For instance, the redox behavior of $–NO_2$ group was explored previously by Zen et al. and Chen et al. during voltammetric estimation of chloramphenicol and parathion respectively [Zen et al., 1999; Chen at al., 2006]. Further, the redox process at bare electrode involves very slow electron kinetics and hence, it requires an appropriate electron mediator on the electrode surface for catalytic improvement. On the surface of bare GCE, a very poor and broad cathodic peak of Azp is observed due to very slow electron transfer kinetics. The modification of GCE with a suitable electron nano-mediator results in improved electrocatalytic activity and the enhanced voltammetric response of Azp. The voltammetric response was enhanced because of Azp adsorption over the composite surface via π- π interaction between the benzene rings of Azp and MoS_2-CPIn. So, the electrochemical behavior of the Azp can be showcased by the following chemical equation:

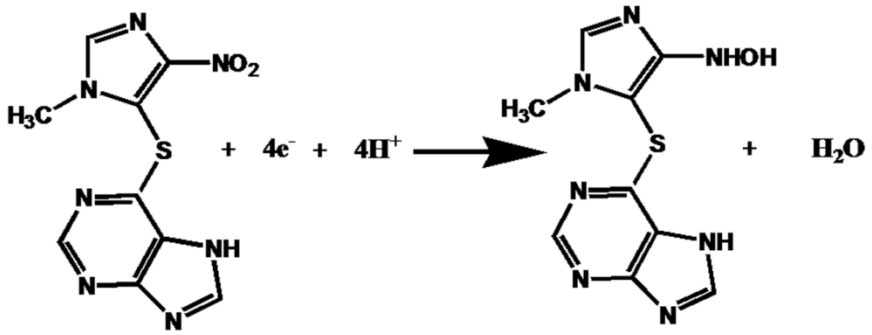

(Eq. 4.5)

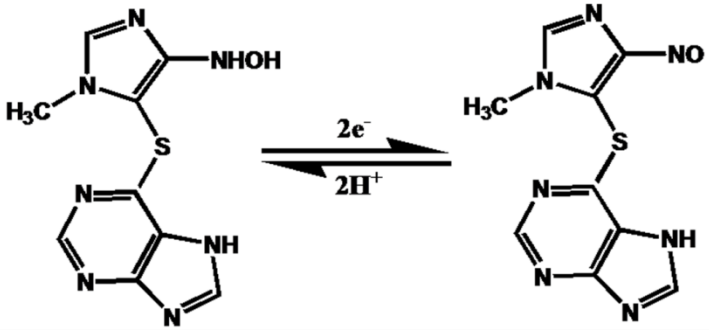

(Eq. 4.6)

4.3.2.2 Optimization of supporting electrolyte pH

CV (Figure 4.6a) and DPV (Figure 4.6b) of 9.9 µM Azp were performed in PBS of different pH (pH= 6.4, 7.0, 7.4 and 8.0) for optimization of pH. The reduction peak current enhances on moving from pH 6.4 to 7.4 and decreases from pH 7.4 to 8.0. This dependency of the Azp reduction peak current over the pH is attributed to the crucial role of protons in the electrochemistry of Azp [Shahrokhian and Ghalkhani, 2009]. So, the supporting electrolyte was decided to be PBS of pH 7.4 at which the maximum current is obtained as a result of the enhanced catalytic activity of the proposed material.

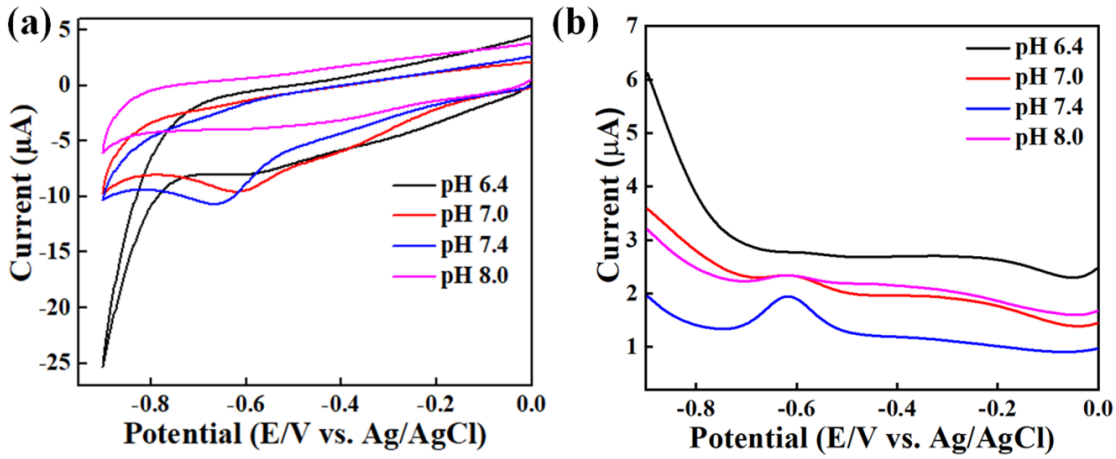

Figure 4.6 (a) CV of Azp (9.9 µM) in 0.1 M PBS over MoS_2-CPIn modified GCE at different pH 6.4, 7.0, 7.4 and 8.0, (b) DPV of Azp (9.9 µM) in 0.1 M PBS over MoS_2-CPIn modified GCE at different pH 6.4, 7.0, 7.4 and 8.0

4.3.2.3 Comparison of different modified electrodes for Azp detection

The MoS_2-CPIn modified GCE did not display any redox peak within the selected potential window (0.0 to -0.9 V) *vs.* AgCl for the blank test sample. So, a suitable potential window was selected such that no redox peak of the material was observed in this range. Electrodes of bare, MoS_2, CPIn, and MoS_2-CPIn modified GCEs were thoroughly investigated for voltammetric responses of 50 µM Azp in PBS of pH 7.4 through CV (Figure 4.7a) and DPV (Figure 4.7b). It is clearly observed that reduction

occurs at the same potential in all the considered cases but the peak current gets varied after different modifications and the current intensity was observed in sequence: Bare <CPIn< MoS_2<MoS_2-CPIn under identical conditions. The result indicates that the composite formed has shown synergism between individual components. In addition, it has a huge surface area and the ability to amplify the electrocatalytic activity of the nanomaterial and it shows remarkable conductivity.

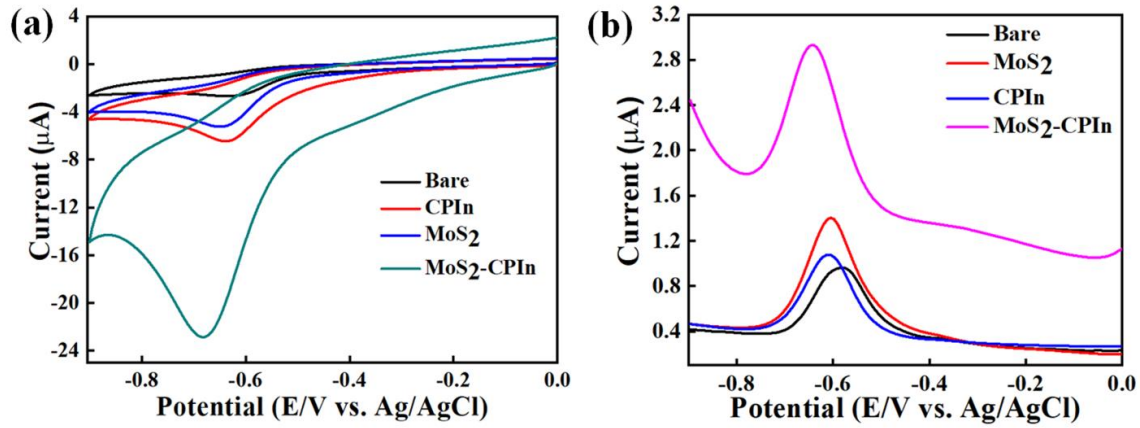

Figure 4.7 (a) CV plots of Azp (50 µM) in PBS (pH 7.4; 0.1 M) over different electrodes, (b) DPV curves of Azp (50 µM) in PBS (pH 7.4; 0.1 M) over different electrodes

4.3.2.4 Voltammetric Sensing of Azathioprine

Under all the optimized conditions, voltammetric experiments were performed for investigating the analytical performance of MoS_2-CPin towards Azp detection using the DPV technique. DPV parameters such as the potential window from 0.0 V to -0.9 V, step potential of 5 mV, modulation amplitude of 25 mV, modulation time of 50 ms, and interval time of 500 ms were chosen to obtain the best signal. Upon successive additions of Azp, well-defined voltammetric responses were recorded in PBS as shown in Figure 4.8(a). On successive addition of Azp, a substantial increment in the reduction peak current depicts a rapid electron transfer reaction over the MoS_2-CPIn modified

electrode, owing to the excellent catalytic effect of the nanostructured platform. The calibration plot in PBS was prepared between Azp concentration and reduction peak current (Figure 4.8(b)). Thus, our sensing platform is extremely sensitive towards Azp estimation and displays a linear current response with a concentration in an extensive range from 3.49 µM to 284.44 µM. The linear regression equation was evaluated as Ipc (Azp) = 0.02379C + 1.55493 with the correlation coefficient R^2=0.99. The sensitivity and LoD of Azp over MoS_2-CPIn modified GCE using DPV technique was determined as 0.33986 $\mu A \cdot \mu M^{-1} \cdot cm^{-2}$ and 74.65 nM respectively.

Detection of Azp in human blood serum is of utmost significance to assess the practicability of the modified electrode for the analyte so that it can be used in diagnostic centers in the future. For this analysis, blood samples were obtained from a healthy person and blood cells were eliminated through centrifugations leaving behind the serum. This serum sample is diluted 10 times using PBS (pH 7.4; 0.1 M). The pH was again checked after dilution in order to assure the final pH of the solution was 7.4. This sample solution did not display any reduction peak at MoS_2-CPIn modified GCE thereby indicating the absence of any reducible compound within the selected potential window. Now, the electrochemical sensing behaviour using the DPV technique was investigated at the modified GCE in the concentration window from 4.00 µM to 98.29 µM and a linear calibration plot was observed (as shown in Figure 4.8(c) & (d)) with an LoD of 195.89 nM with 0.29557 $\mu A \cdot \mu M^{-1} \cdot cm^{-2}$ sensitivity (S/N: 3). Now, the detection of Azp was investigated in spiked human serum samples using a similar dilution procedure and PBS of pH 7.4. The recovery study of the developed sensor has been investigated using the standard addition method. The standard solution of Azp was added to the test solution and the calibration plot was utilized for the quantitative

estimation of Azp. The results obtained from three serum samples are listed in Table 4.1 and values demonstrate a good recovery of results. The proposed sensor with obtained results of the analytical parameters was compared with that of the previously reported Azp sensors and presented in Table 4.2. The observed results suggest that the proposed sensor can effectively be used for the quantitative estimation of Azp in real sample analyses.

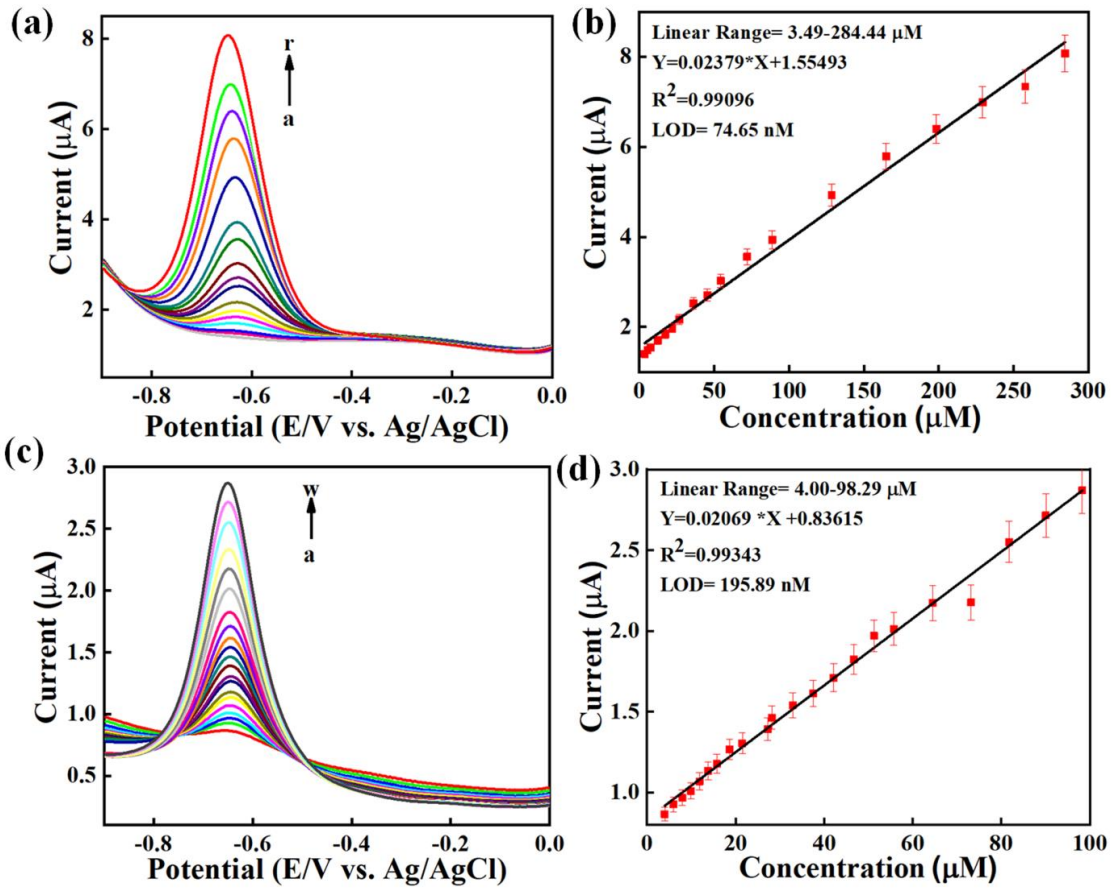

Figure 4.8 DPV measurements of various concentrations of Azp (3.49-284.44 μM) (a-r) using MoS_2-CPIn modified GCE in PBS (pH 7.4; 0.1 M), (b) linear calibration plot of Azp in PBS (pH 7.4; 0.1 M). (c) DPV responses of different concentrations of Azp (4.00-98.29 μM) (a-r) using MoS_2-CPIn modified GCE in human blood serum, (d) linear calibration plot of Azp in the human blood serum sample

Table 4.1 DPV detection of Azp in spiked blood serum samples

Blood Serum Samples	**Spiked (µM)**	**Detected* (µM)**	**Recovery (%)**
Sample A	11.80	11.40	96.61
Sample B	46.75	47.78	102.20
Sample C	90.09	90.79	100.78

*Mean average of three estimations.

Table 4.2 Comparison with earlier reported studies for electrochemical detection of Azp

Modified Electrode	**Technique**	**Supporting electrolyte**	**LoD (µM)**	**Linear-Range (µM)**	**Matrix**	**Reference**
NDG/CS/GCE	CV	PBS	0.065	0.2-100	Human blood serum &Pharmaceutical formulation	[Shahrokhian and Ghalkhani, 2010]
Au/Au-NA	DPV	PBS	0.090	0.095 - 900	Pharmaceutical formulation	[Vaisa et al., 2015]
CNP/N/GCE	CV	PBS	0.080	0.2 - 2	Human blood serum &Pharmaceutical formulation	[Shahrokhian and Ghalkhani, 2015]
AgNPs-G/PGE	CV	PBS	0.068	0.7-100	Pharmaceutical formulation	[Asadian et al., 2016]
G-CS/GCE	SWV	PBS	0.047	0.1 - 26	Human blood serum &Pharmaceutical formulation	[Hatami and Jalali, 2015]
MoS_2-CPIn	DPV	PBS	0.074	3.49-	Human blood	[Present

				284.44	serum	work]

NDG= Nano diamond-graphite, CS= Chitosan, Au-NA= Gold hierarchical dendrites of pyramidal nanoparticles, CNP= Carbon nanopartilces, N= Nafion, G= Graphene, PGE= Pyrolytic graphite electrode , MWCNTs= Multi-walled carbon nanotubes , MCs=Microcubes,

4.3.2.5 Selectivity and Interference study of the proposed sensor

While designing a sensor, selectivity and cross-reactivity studies are of utmost importance because complex test samples contain many other bio components like lipids, carbohydrates, etc. that can hinder the detection of the desired analyte. So, the selectivity of our proposed sensor for Azp detection was investigated with some common biologically important molecules that are present in human blood like L-ascorbic acid, cholesterol, creatine, DA, glucose, glycine, UA and urea and as shown in Figure 4.9. The concentration of all the interferants was chosen 10 times higher than the Azp concentration. The percentage interference was calculated to be 5.39 % for L-ascorbic acid, 7.87 % for cholesterol, 2.99 % creatine, 3.14 % for glucose, 4.33 % for glycine, 9.88 % for urea, 5.85 % for UA, and 12.79 % for DA respectively and clearly, all of them showed very less or negligible interference. It was clearly demonstrated that our proposed electrochemical sensor showcased a high selectivity towards Azp detection.

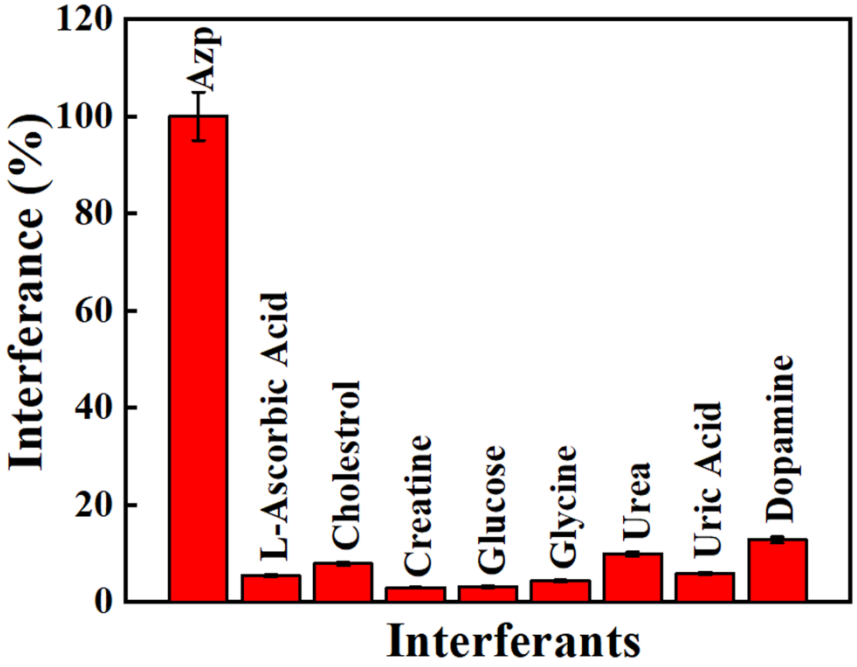

Figure 4.9 Interference study. The x axis denotes the tested compounds and the y axis denotes the interference effect in percentage (%)

4.4 Conclusion

In conclusion, we have illustrated an easy and successful synthesis of 5CPIn decorated MoS_2 nanosheets for the development of an electro-sensing platform as a modified GCE. This work offers a simple, cost-effective, and sensitive electroanalytical estimation of Azp in the biological sample without any cross-reactivity, false positives and matrix complications. The LoD was achieved to be as low as 74.65 nM. This method does not need any pre-treatment of the sample. The ultra sensitivity of this nanomediator can be assigned to the immensely huge surface area, magnificent electrical conductivity and rapid electrode kinetics due to the electrocatalytic effect. Based on this sensing performance in PBS and blood serum, it can be concluded that the present methodology has immense potential to be effectively applied for the quantitative estimation of Azp in pharmaceutical formulations.